CARBON 53 (2013) 50–61

Available at www.sciencedirect.com

SciVerse ScienceDirect

journal homepage: www.elsevier.com/locate/carbon

Improvement of the mechanical properties of single-walled carbon nanotube networks by carbon plasma coatings

Antti Kaskela [a,*], *Jari Koskinen* [b], *Hua Jiang* [a], *Ying Tian* [a], *Xuwen Liu* [b], *Toma Susi* [a], *Markus Kaukonen* [a], *Albert G. Nasibulin* [a], *Esko I. Kauppinen* [a]

[a] *NanoMaterials Group, Department of Applied Physics and Center for New Materials, Aalto University, P.O. Box 15100, 00076 Espoo, Finland*
[b] *Department of Materials Science and Engineering, Aalto University, P.O. Box 15100, 00076 Espoo, Finland*

ARTICLE INFO

Article history:
Received 3 February 2012
Accepted 10 October 2012
Available online 22 October 2012

ABSTRACT

Carbon vacuum arc was used to deposit 5–25 nm thick carbon coatings on single-walled carbon nanotube (SWCNT) networks. The SWCNT bundles thus embedded in conformal coatings maintained their optical transparency and electrical conductivity. Sheet resistances of the networks were measured during the vacuum arc deposition, revealing initially a 100-fold increase, followed by significant recovery after exposing the samples to an ambient atmosphere. Nanoindentation measurements revealed improved elasticity of the network after applying the carbon coating. Pristine SWCNT networks were easily deformed permanently, but a 20 nm carbon coating strengthened the nanostructure, resulting in a fully elastic recovery from a 20 μN load applied with a Berkovich tip. In nano-wear tests on selected areas, the coated SWCNT maintained its networking integrity after two passes raster scan at loads up to 25 μN. On the other hand, the pristine networks were badly damaged under a 10 μN scan load and completely displaced under 25 μN. Raman and electron energy loss spectroscopies indicated the carbon coating on bundles to be mainly sp^2 bonded. Finite element modeling suggests that the low content of sp^3 bonds may be due to heating by the intense ion flux during the plasma pulse.

1. Introduction

Carbon nanotubes possess unique electrical and mechanical properties, which make them potentially applicable as networks and thin films. Yet the functional thin films have very modest mechanical strength when compared to hard nanostructured thin films [1]. Specifically, single-walled carbon nanotubes (SWCNT) and their networks can be used as transistors, optically transparent conductors for conventional and flexible electronics, sensors, acoustical emitters, *etc.* by using simple and straightforward synthesis and deposition approaches [2–7]. Optically transparent electrodes are one of the most promising application areas and provide large commercial and technological potential due to the abundance of raw materials and the superior flexure resistance of SWCNT networks compared to conventional transparent electrode materials, such as ITO [8]. However, SWCNT networks can be prone to mechanical damage from scratching and wear, and therefore an improvement of their mechanical properties would be beneficial for a variety of applications requiring exposed SWCNT networks [9]. The reported yield strength of SWCNT networks is some tens of MPa, [10] which is about three orders of magnitude lower than that of hard nanostructured coatings [1]. Protective coatings of diamond-like carbon have long been used to improve the wear resistance of bulk materials [11]. This lead us to hypothesize that similar carbon coatings could provide a way to covalently bond together SWCNTs in networks to improve their mechanical perfor-

* *Corresponding author.*
E-mail addresses: Antti.Kaskela@aalto.fi (A. Kaskela), Jari.Koskinen@aalto.fi (J. Koskinen).
0008-6223/$ - see front matter © 2012 Elsevier Ltd. All rights reserved.
http://dx.doi.org/10.1016/j.carbon.2012.10.016

mance, while preserving their native electrical conductivity and optical transparency.

Coating of carbon nanostructures by using carbon ion or plasma beams has rarely been discussed in the literature. Hydrogen-containing diamond-like carbon (DLC) films have been grown on top of dense aligned MWCNT forests and on spin-coated CNT dispersions by plasma chemical vapor deposition (PCVD) [12,13]. The mechanical strength and hydrophobic properties of the MWCNT forests were enhanced [13]. Schittenhelm and co-workers utilized a pulsed laser deposition (PLD) carbon coating process with ion energies of around 100 eV on SWCNT bundles, and were able to maintain metallic conduction while increasing the scratch resistance of the films [14]. However, none of the aforementioned papers provides detailed atomic scale characterization of the structure of the carbon coating.

In this work, we describe the synthesis of a composite nanomaterial composed of a non-hydrogenated PVD carbon coating of a SWCNT network. The material is characterized using transmission electron microscopy (TEM), scanning electron microscopy (SEM), electron energy loss spectroscopy (EELS) as well as Raman and optical absorption spectroscopy. Additionally, the improvement of the mechanical properties of the hybrid nanomaterial is evaluated by comparison to pristine SWCNT network using a nanoindentation technique. We also report for the first time a physical vapor deposition (PVD) carbon coating applied to freestanding SWCNT networks, i.e. networks without a supporting substrate. Carbon coatings are grown on the SWCNT networks by applying a pulsed vacuum arc discharge deposition, with the growth process monitored by *in situ* sheet resistance measurements.

2. Experimental

SWCNTs were synthesized using a high temperature catalytic aerosol CVD process, which is based on the thermal decomposition of ferrocene, subsequent formation of iron nanoparticles, and the catalytic decomposition of carbon monoxide on the surface of iron nanoparticles leading to SWCNT formation [15]. Subsequently, the SWCNTs spontaneously bundle and form aggregates from a few to tens of parallel SWCNTs to minimize their surface free energy [16]. The formed SWCNT bundles are on average 9 μm in length and about 12 nm in diameter, as determined by statistical analysis of SEM and TEM images of the reaction products described elsewhere [6]. SWCNTs are collected in the form of randomly oriented networks at the outlet of the synthesis reactor using nitrocellulose membrane filters (Millipore Ltd. HAWP, 0.45 μm pore size). By varying the deposition duration, the amount of deposited SWCNT bundles and thus the thickness of the samples can be varied from sub-monolayer SWCNT bundle coverage to thick multilayered SWCNT networks up to a few micrometers in thickness [6,7]. Samples were further transferred onto substrates, or formed free-standing SWCNT networks with a dry room temperature press transfer process, described in detail elsewhere [6,7]. Thin sub-monolayer samples consisting of sparsely deposited SWCNT bundles were deposited on TEM grids (Holey Carbon Film 400 Mesh CU, Agar Scientific, UK) by placing the TEM grids on a nitrocellulose filter for a 15 s deposition.

The carbon coatings were deposited using a pulsed vacuum arc without energy filtering. A 2.6 mF capacitor bank was charged to 200 V and the arc was triggered with ignition electrodes. The maximum pulse current was 3 kA and the pulse half width was about 150 μs. Each pulse was triggered separately at 1 Hz frequency. The deposition rate during the pulse was about 1.4×10^{15} ions/cm^2, as measured from the growth rate of a carbon layer on a flat silicon substrate. The distance from the cathode was about 300 mm. The average carbon ion energy has been measured to be 40–50 eV using an electrostatic probe [17]. It may be assumed that all carbon in the plasma is ionized [18].

For *in situ* electrical resistance characterization, a rectangular SWCNT sample was prepared on a polymer surface (PET, 125 μm thick, Sigma–Aldrich). Copper conductors were attached to both ends of the sample area using commercially available silver paint, and connected to an external multimeter (Fluke 88). In addition, the sample was measured after the coating process to study the impact of ambient doping and the subsequent recovery of sheet resistance. To extract electrical characteristics of pristine and carbon coated SWCNT samples on PET and Si substrates, a four point probe and a digital multimeter were used for the sheet resistance measurements (Jandel four-point probe, Jandel Engineering Ltd./Agilent 34411, Agilent).

Structural characterization of the coating microstructure was done using a field emission TEM with double-Cs aberration correctors (JEOL JEM-2200FS operated at 80 kV). Furthermore, Raman and optical absorption spectroscopies characterized the electronic structure of the samples. TEM grids with pristine or carbon-coated SWCNT bundles were investigated with a Raman spectrometer (Wintech Alpha300). Raman spectra were collected using a frequency-doubled Nd:YAG green laser (λ = 532.25 nm). For micro-Raman measurements, an Olympus 100× air objective was used leading to laser spot size of about 200 nm, while the sample was maintained at room temperature. The location of SWNCT bundles was determined by mapping the integrated intensity of the nanotube/graphite-specific G band, from 1550 to 1620 cm^{-1}, and by extracting the Raman signal from spatial areas exhibiting a high SWCNT-related G band intensity. Large area samples on $Si/Si0_2$ substrates used for nanoindentation were characterized by stationary Raman measurements. As the silicon substrate used for nanoindentation doesn't allow optical absorption spectroscopy in a transmission configuration, separate samples were fabricated on transparent PET substrates for optical absorption spectroscopy, which was performed using a dual beam spectrophotometer (Perkin–Elmers Model 950).

To study the mechanical behavior of the SWCNT structure, a SWCNT bundle network, with thickness of about 200 nm, as estimated based on optical absorption [7] in thickness was transferred onto a silicon wafer. The SWCNT network with a pristine sheet resistance of 100 Ω/sq. and an optical transmittance of 50% (at 550 nm) was selected to provide similar sheet resistance characteristics as typical commercially available ITO-on-polymer transparent conductors to test the viability of the carbon coated SWCNTs as an alterative

material. An approximately 20 nm thick carbon coating was then applied on part of the network. Then, indentation was carried out with a TriboIndenter® TI-900 (Hysitron, Inc.) nanomechanical testing system. A load-control mode was used in the measurement in which arrays of indents with varying maximum loads were performed on selected areas on both the coated and uncoated SWCNT with the peak-load range varied from 20 to 200 μN. The indenter was a Berkovich-type with a nominal tip radius of 130 nm.

The nanowear experiments were designed to test the mechanical response of the SWCNT bundles under contact pressure. In the nanowear experiments, a Berkovich tip scanned a selected area on the sample surface with a set of speed of 2.4, 5 and 10 nm/s to scan an area of 2.4×2.4, 5×5 and 10×10 μm, respectively. The load for scan wear was constant at 10 and 25 μN. A larger region containing the worn area was then imaged with a load of 0.5 μN. Trial-scan before the nanowear experiments had shown that on both of the coated and uncoated sample the surface change was negligible under this small load. The worn surface on the coated and non-coated network was examined by studing the scanning probe microscopy SPM images in assistance with SEM observation. The amount of wear and material deformation/displacement was estimated by comparing the 3D-reconstructions of surface profiles before and after the nanowear experiments.

3. Results and discussion

In the PVD carbon coating 250 pulses were applied on the exposed SWCNT bundle surfaces (equivalent to approximately 25 nm thick layer). SEM observation revealed that in the uniform layer blanketing the network surface, the carbon seemed selectively applied on the bundle threads, thickening them and partially covering the holes of the network (Fig. 1). The basic interconnected structure of the network was maintained despite the harsh coating process. Manually performed light mechical scratching of the PVD-coated SWCNT network revealed clear morphological difference between the coating modified, crust-like, heavily interconnected top-layer and the non-modified underlying SWCNT network (Fig. 1c). Formation of this heavily interconnected top layer can be explained by process in which the PVD coating deposits on bundles near the surface and gradually reduces the empty area between the bundles leading to a progressively more localized deposition at the surface, while the lower SWCNT layers are shadowed by the top layers and stay largely unmodified by the coating. The surface-localized coating is evident also when comparing the side-views of the ethanol densified, non-coated network and it's PVD-coated counterpart in the Fig. 1d and e. The cross-sectional imaging was performed by mechanically peeling small flakes of the networks away from the substrate and by imaging these relatively well-defined flakes at approximately perpendicular direction by tilting the SEM sample stage.

Fig. 2 shows a photograph of the freestanding carbon-coated SWCNT network with the same coating thickness on a 200 nm thick SWCNT network, clearly demonstrating the optical transparency of the hybrid material. The freestanding SWCNT network was coated and analyzed without the ethanol densification, which leads to different bundle morphology when compared to densified samples, which were discussed previously and are later analyzed with nanoindentation and nanoscratching measurements. As ethanol densification changes the film morphology from a highly porous 3d-structure to a dense 2d-structure, the pristine films exhibit more separated small diameter bundles both prior and after the coating process, allowing statistical estimation of the bundle diameter increase due to the PVD coating process. The diameter increase of SWCNT bundles due to the coating process is readily observed from the SEM images (Fig. 2b and c). The average bundle diameter increases from (12 ± 6) to (73 ± 14) nm during the coating process.

The structural modification of the bundle surfaces is observable by TEM imaging of the pristine and PVD-coated small diameter SWCNT bundles with a thinner PVD coating of 50 pulses (about 5 nm), depicted in Fig. 3a and b, respectively. The clean and well-defined tubular bundle surface of pristine SWCNTs is transformed to wavy and defective structures surrounding the bundles. In the inner part of the bundle, SWCNTs are still observed, indicating that at least the innermost SWCNTs are preserved during the coating process. Interestingly, the TEM images reveal that the carbon coating has a partially crystalline structure, with a graphitic interlayer separation. Smaller diameter bundles depicted in the figures Fig. 3c and d suggest surface localized damage leading to more severe deterioration in small diameter structures. Mass addition due to the coating can be estimated based on the bundle diameters and the SWCNT bundle and coating densities. Typical reported values are for SWCNT bundle density 1.3–1.4 g/cm^3 and for carbon coatings 2.5–3.0 g/cm^3. For typical TEM-imaged samples depicted in Fig. 3a and b, consisting of SWCNT bundles (10 nm diameter, density 1.3 g/cm^3) coated with 50 plasma pulses (5 nm, density 2.5 g/cm^3) this would correspond mass increase of approximately 250%. The structure is drastically different from prior work with macroscopic solid substrates with similar PVD process parameters, which yielded mainly sp^3-configured amorphous diamond-like carbon (DLC) coatings [17].

Typical sheet resistance characteristics for a thin SWCNT sample during the carbon plasma coating is shown in Fig. 4. The sample was measured in an ambient atmosphere prior to placing it in the vacuum chamber. Desorption of ambient adsorbents increases the sheet resistance of the sample during vacuum exposure prior to the PVD coating process. The sheet resistance increases by about one order of magnitude during the first ten coating pulses. The increase of sheet resistance can be partly attributed to further desorption of air species like H_2O and O_2, as the sheet resistance largely recovers when the sample is exposed to ambient conditions after the coating process. A 5-fold increase of the sheet resistance persists after half a year of storage in ambient conditions, indicating coating-induced permanent defects or increased bundle-to-bundle contact resistances. Sputtered carbon atoms in intertube and interbundle contacts could cause increased contact resistances. While the electrical performance of this thin and highly transparent SWCNT film (90% at 550 nm) is degraded during the coating process, the compos-

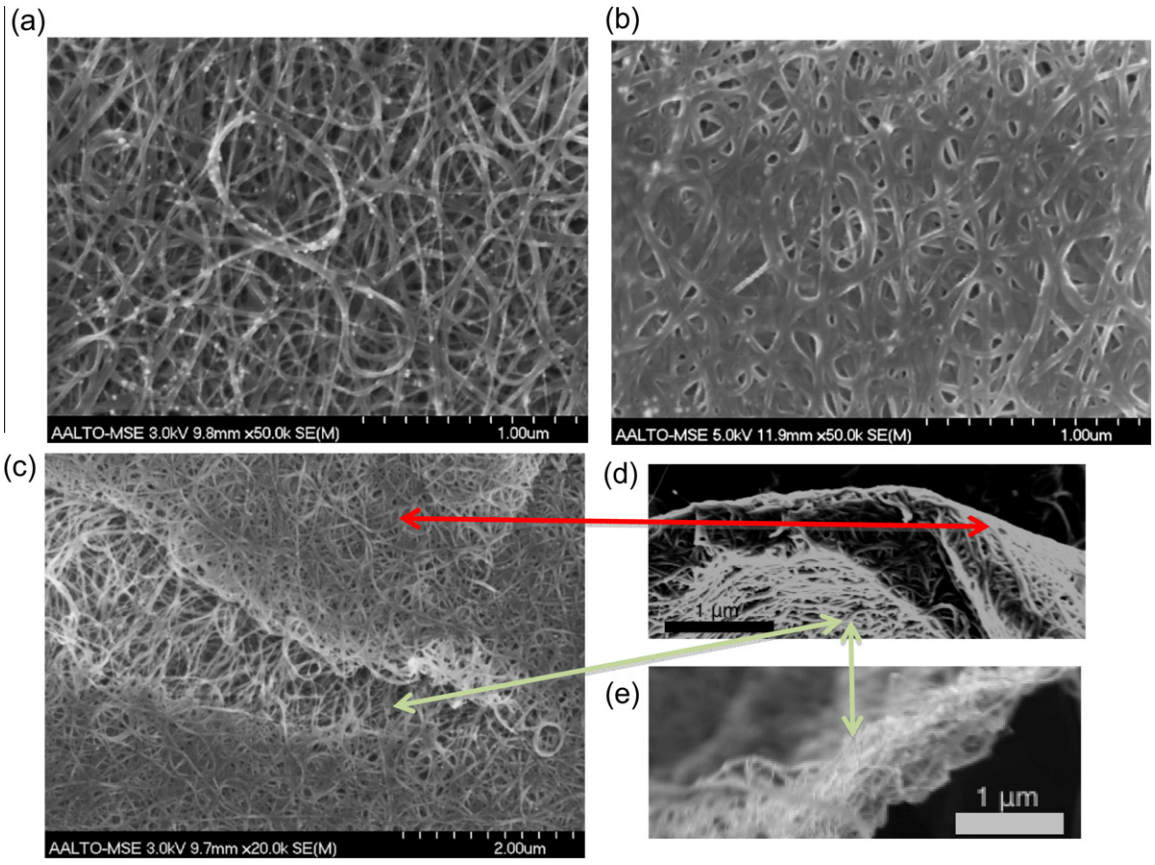

Fig. 1 – SEM images of (a) an ethanol densified SWCNT network and (b) an ethanol densified, PVD-coated SWCNT hybrid nanomaterial (c) a macroscopic scratch, which reveals a crust-like, highly interconnected, coating modified SWCNT network near the top-surface of the sample, and underlying pristine SWCNT-network, (d) a cross sectional view of the PVD-coated network (indicated by the red arrow) and (e) the non-coated densified SWCNT-network (indicated by green arrows), showing the effects of carbon PVD coating to the morphology of the SWCNT network. (For interpretation of the references to color in this figure legend, the reader is referred to the web version of this article.)

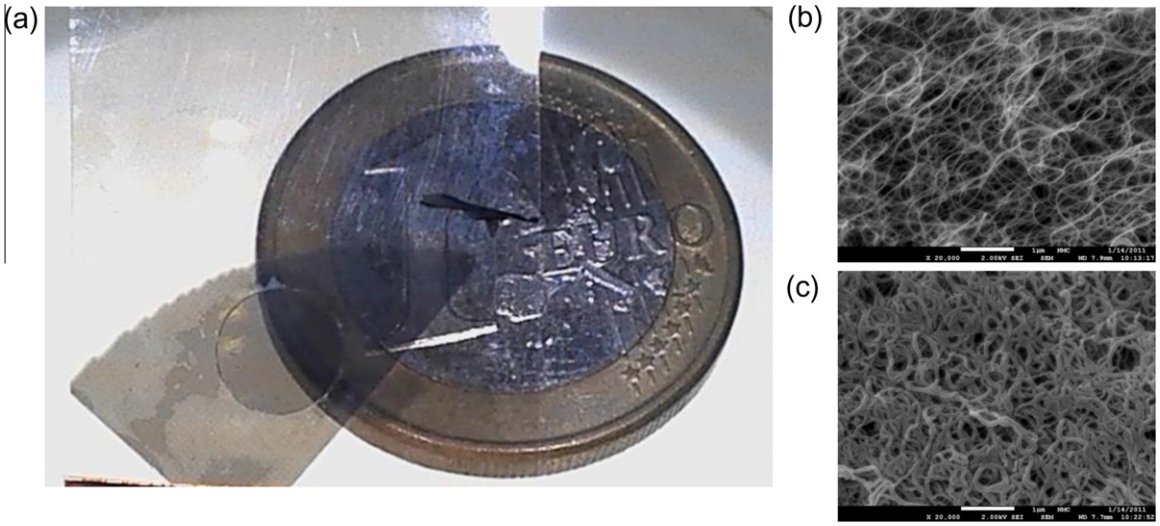

Fig. 2 – (a) A freestanding PVD-coated SWCNT film with carbon coating extends over the circular opening in the PET substrate, demonstrating the optical transparency of the formed hybrid nanomaterial. (b) The freestanding network was fabricated without ethanol densification, leading to clearly separated bundles both prior and (c) after the coating process, thus allowing statistical estimation of diameter increase of the bundles during the coating process.

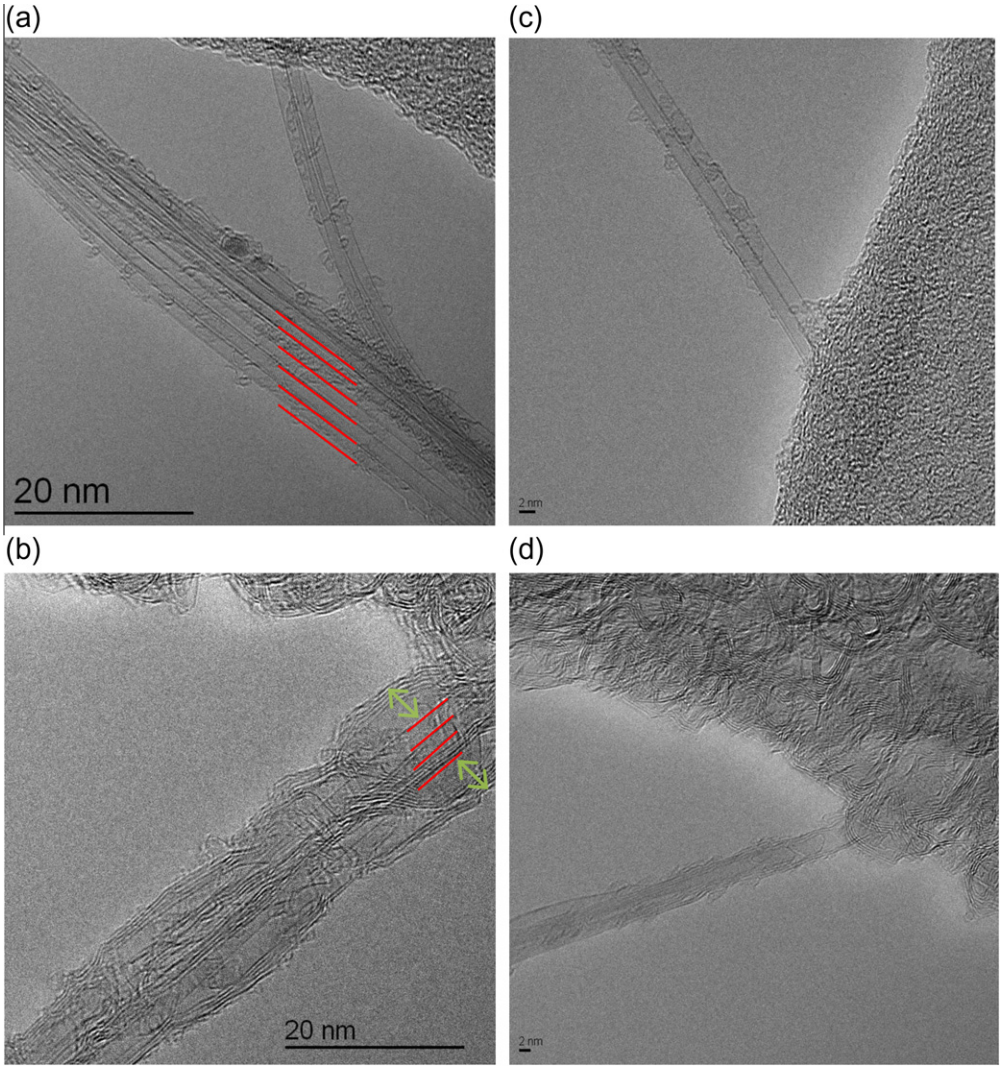

Fig. 3 – TEM images of (a) pristine SWCNTs and (b) the carbon-coated SWCNT hybrid nanomaterial after 50 PVD coating pulses. Red lines in the images highlight the location and directions of SWCNT sidewalls in the bundles and the green arrows highlight the location of deposited carbon coating. Figures (c) and (d) depict pristine and carbon coated surfaces of small diameter bundles, respectively, The carbon coated bundle exhibit a less pronounced core–shell structure, which can be explained by localized damage near the surface. (For interpretation of the references to color in this figure legend, the reader is referred to the web version of this article.)

ite structure still maintains significant electrical conductivity after the plasma coating process.

Optical absorption spectroscopy suggests that the characteristic absorption bands of semiconducting and metallic nanotubes are maintained during the carbon plasma coating process as shown in Fig. 5. The sample with a thin carbon coating exhibits only a small absorption change at the low wavelength π-plasmon peak of the spectrum, which is related to the increased total carbon content of the sample, also observable in the absorption spectrum of only carbon coated PET-substrate. The positions of the nanotube-specific transitions are unaffected, indicating that the carbon nanotubes survive the coating process. The optical absorbance at the 550 nm wavelength is 50% and 40% for the pristine and carbon coated SWCNT networks, respectively. In order to justify the claim of the material as transparent and conductive, also the electrical characteristics were measured. Sheet resistances of 100 Ω/□ and 220 Ω/□ were observed for pristine SWCNTs and carbon coated SWCNTs. The same effect was also verified for samples on Si-substrates, which were later used for mechanical testing. Therefore the hybrid material consisting of a carbon coating on SWCNT network can be claimed to be optically transparent and electrically conductive.

A typical electron energy loss spectroscopy (EELS) spectrum, presented in Fig. 6, exhibits a slight increase in the intensity of the energy step starting at 290 eV, indicating increased sp^3-bonding fraction [19]. An increase in the ratio of the areas under the sp^2-related peak around 285 eV and the energy step between 290 and 305 eV is not as high as could be expected for sp^3-bonded carbon in DLC coatings deposited on macroscopic surfaces such as Si (100) [19]. Rather, EELS

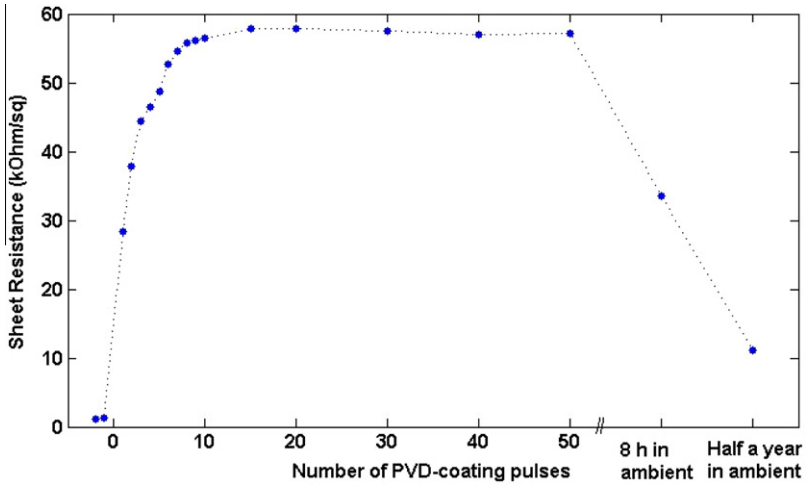

Fig. 4 – *In-situ* measurement of a thin, highly transparent SWCNT network sheet resistance during the PVD carbon coating process. The increase of sheet resistance stabilized after 10 pulses and recovers significantly after the sample is exposed to ambient conditions.

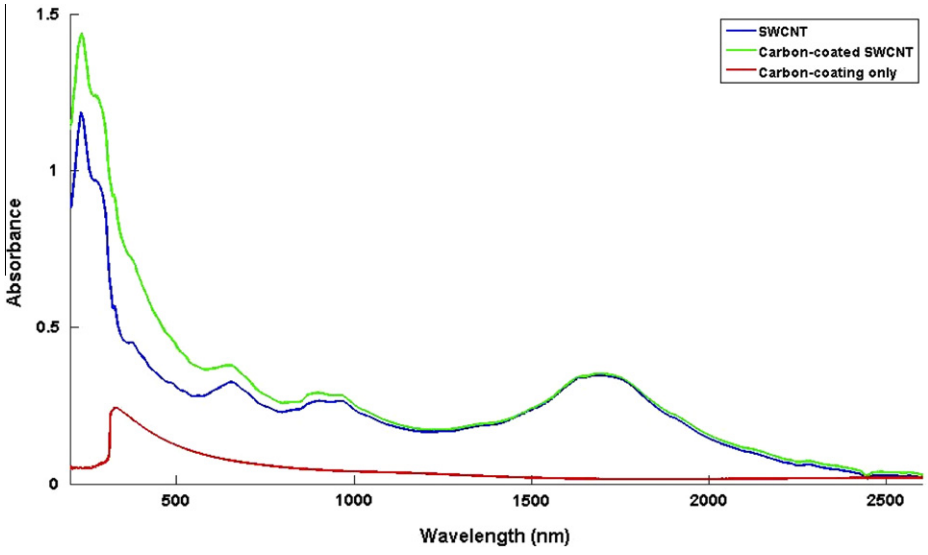

Fig. 5 – Optical absorption spectra of pristine (blue), carbon coating without SWCNTs (red) and carbon-coated (green) SWCNT networks. Increasing absorbance around the π-plasmon peak indicates increased sp^2 bonded carbon content after coating. (For interpretation of the references to color in this figure legend, the reader is referred to the web version of this article.)

suggests that a significant fraction of the carbon atoms in the coating are sp^2-configured, which could indicate that the formation of a carbon coating on a nanostructured surface exhibits anomalous behavior. This can originate from a relaxation mechanism that leads the carbon bonds to reconfigure to an energetically more stable sp^2-hybridization. However, a quantitative determination of sp^2/sp^3 ratio based on EELS-spectra is challenging due to overlapping SWCNT and amorphous carbon signals. Raman spectra, which are depicted in Fig. 7, further indicate that SWCNTs in small diameter bundles do survive the coating process. The Raman signal of the coated sample exhibits a slightly decreased G/D ratio, indicating slightly increased disordered sp^2-hybridized carbon content. Raman measurements on Si substrate verified the results for samples that were used for the mechanical testing and had both thicker SWCNT and carbon coating layers, providing similar results to micro-Raman characterized samples on TEM-grids. The samples with only a carbon coating on Si substrate exhibits a broad, small intensity G-band signal typical for DLC-coatings [19].

To assess the possibility of bond reconfigurations due to heating of the SWCNT bundle, we used finite element modeling (COMSOL Multiphysics 4.2). In the model the fiber was heated from one end while the other was at a heat sink. During the pulse, heat flux due to the ions is of the order of 1 MW/m^2. Assuming a SWCNT bundle 12 nm in diameter, and a distance of 9 μm with one end connected to a heat sink at 300 K, the maximum temperature of the fiber was calculated. It may be assumed that the heat conductivity of the SWCNT bundle is significantly lower than the theoretical maximum of

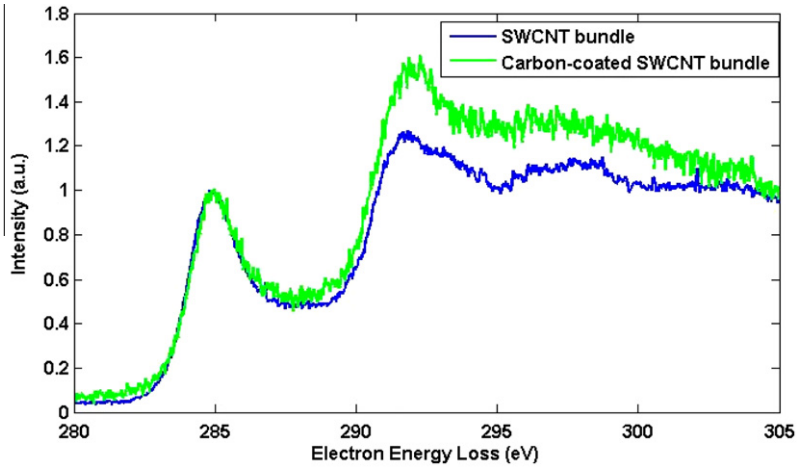

Fig. 6 – Electron energy loss spectra measured on pristine (blue) and carbon-coated (green) SWCNT bundles. (For interpretation of the references to color in this figure legend, the reader is referred to the web version of this article.)

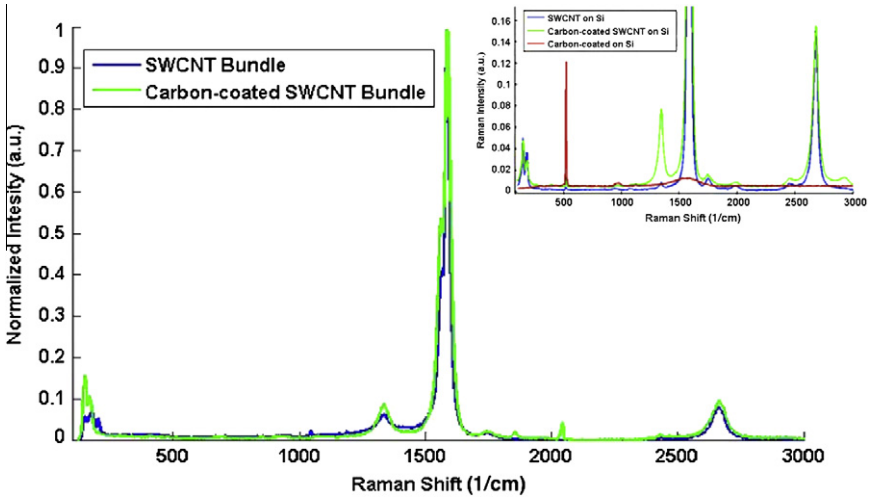

Fig. 7 – Normalized Raman spectra of pristine (blue) and carbon-coated (green) SWCNT samples measured with the micro-Raman set-up. The inset shows the Raman spectrum of the carbon coating on a Si substrate, exhibiting diamond-like carbon characteristics around at 15501/cm. SWCNT and carbon-coated SWCNT samples exhibit similar characteristics both in micro- and macro-Raman measurements. (For interpretation of the references to color in this figure legend, the reader is referred to the web version of this article.)

3500 W/mK [20]. However, even with a thermal conductivity 3 W/mK, a temperature rise of less than one degree occurs. But if no contact to the heat sink is assumed, the maximum temperature is over 1000 K. Given the porous structure of the SWCNT networks and the poor intertube, interbundle and bundle-to-substrate heat coupling, it is justified to expect extremely high local temperatures during the coating cycles. This could lead to the thermal relaxation of sp^3 bonding to energetically more favorable sp^2 bonding. It is known that the deposition temperature has a strong effect on the bonding structure of carbon films. On a solid substrate, a carbon film deposited at a substrate temperature below 400 °C has an sp^3 content of over 60%, while above 500 °C the coating is predominantly sp^2-bonded [17]. A 20 nm carbon film deposited with identical deposition parameters on Si (100) was confirmed to be ta-C, as expected, by obtaining an atomic density of about 3.0 g/cm^3 with X-ray reflectivity measurement [19,21]. We thus suggest that the heat flow controlling the temperature during the growth of the carbon film on the SWCNT bundles has a key role in determining the bonding structure of the coating.

It is known that mechanical loading can permanently deform SWCNT networks, which can be detrimental for the mechanical durability of SWCNT network devices. Fig. 8 presents wear patterns of worn surfaces from the carbon coated and non-coated networks. Three scans performed on three concentric areas starting from a size of 15×15 μm then 10×10 μm and finally 5×5 μm with the corresponding scan loads of 1, 10 and 25 μN, respectively. For the non-coated network, the post-scan SPM image (Fig. 8a) does not reveal clear frames from the scan wear, but rather a roughened surface. However, the three scan frames are clearly visible from the

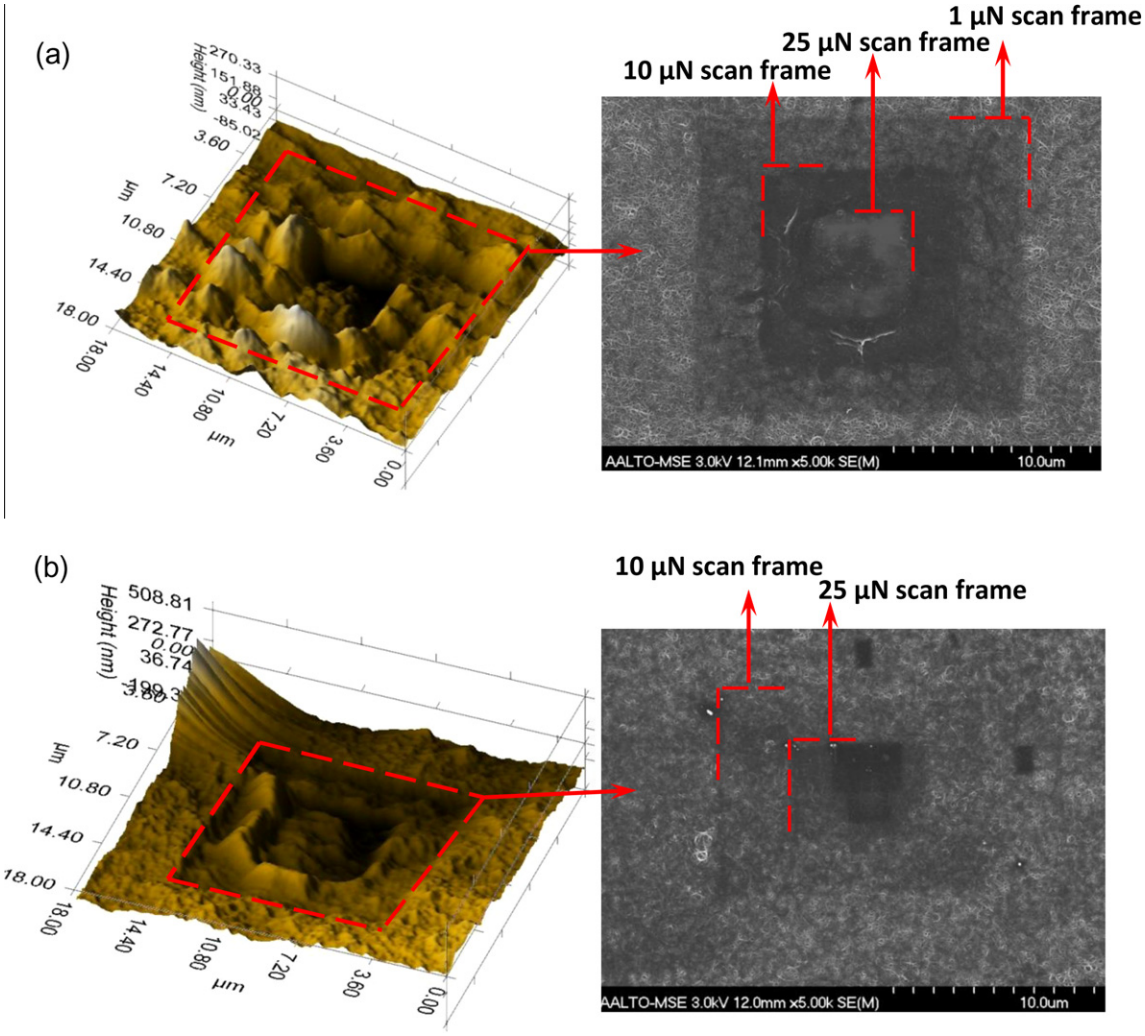

Fig. 8 – SPM and SEM images of worn (a) non-coated and (b) carbon coated SWCNT networks by scan-wear tests at different loads (the small dark rectangle-shaped frames are caused by SEM-electron beam when focusing at higher magnifications). The coated network is more resilient and wear resistant than the non-coated one.

SEM image. It can be seen that even at a 1 μN force the tip left permanent deformation on the network surface. As the load increased to 10 μN, the network is completely smeared, and then largely removed with the 25 μN load. The carbon coated network, on the other hand, exhibited higher resilience as only the 25 μN scan frame is clear while the 10 μN scan frame is hardly seen and the 1 μN frame is invisible. Therefore, the network maintained its integrity after multiple wear scans (Fig. 8b). The dark rectangles shaped frames in Fig. 8b were caused by the electron beam contamination during focusing at higher magnifications. Here, it should be understood that the SPM images generated from a blunt tip (>130 nm tip radius) will not be able to reveal the details of the network bundles. Still, the SPM images demonstrate that the network bundle became much smoother after the carbon coating (comparing Fig. 8a to 8b).

To estimate the amount of wear loses or material deformation/displacement, a separate scan wear test was performed and results are shown in Figs. 9 and 10. It is clear that the topography of the non-coated surface has been transformed totally (Fig. 9a and b) and the worn region is clear outlined (Fig. 9c). For the carbon-coated sample the surface topography still resembles the original one after the nanowear test (Fig. 10a and b) with a faint frame indicating the worn region (Fig. 10c). The estimated volume of the worn area is 3.4 μm^3 for the non-coated and 1.4 μm^3 for the carbon-coated sample. The average depth of the worn region is about 120 nm for the non-coated and 45 nm for the carbon-coated samples.

The typical load-displacement curves from nanoindentation measurement also demonstrate the resilient mechanical behavior of the coated SWCNT network (Fig. 11). Here, the peak load was so chosen that the corresponding indent depth was less than the nominal network thickness so that the mechanical response would reflect the network-only behaviors with minimal substrate effects. As can be seen, the coated network not only demonstrates higher resistances to indenter penetration but also larger elastic recovery. In Fig. 11, the ratio of the recovered depth to the maximum depth at the two corresponding peak-loads is calculated by the equation: $(h_{max} - h_r)/h_{max}$, where h_{max} is the correspond-

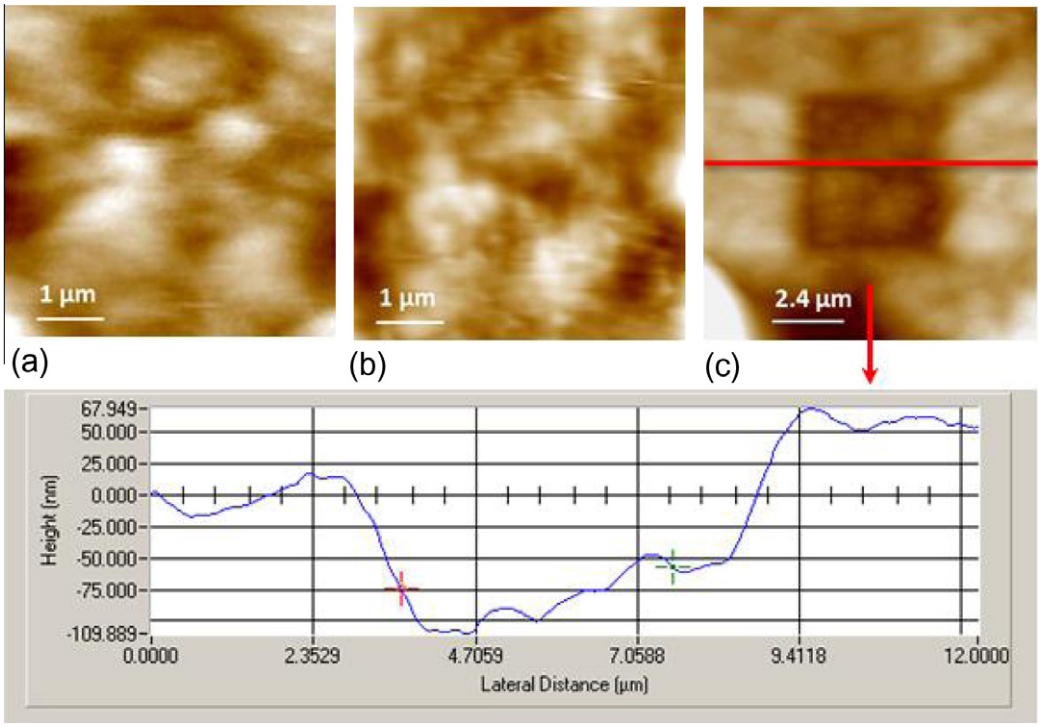

Fig. 9 – SPM images of the non-coated SWCNT network on silicon in the nanowear test: (a) Original surface topography at the selected area of 5 μm^2, (b) after nanowear under a 10 μN load, and (c) a larger area image highlighting the worn region. A line-scan crossing the red line in image (c) shows the surface profile. (For interpretation of the references to color in this figure legend, the reader is referred to the web version of this article.)

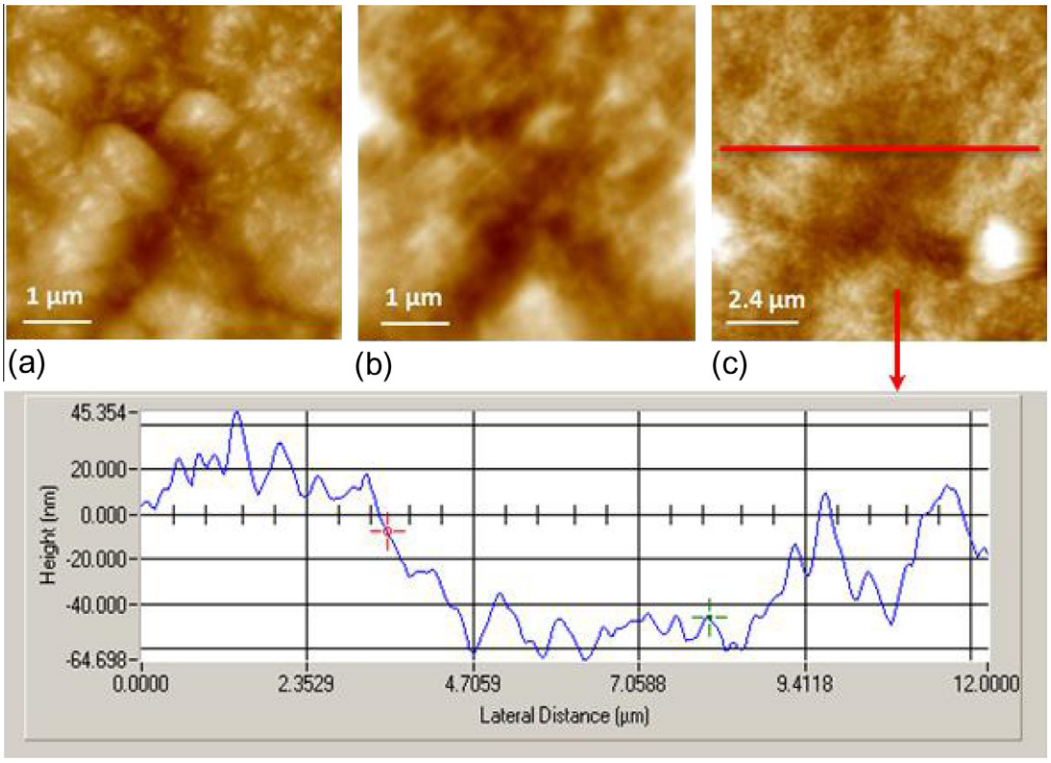

Fig. 10 – SPM images of the coated SWCNT network on silicon in the nanowear test: (a) Original surface topography at the selected area of 5 μm^2, (b) after nanowear under a 10 μN load, and (c) a larger area image highlighting the worn region. A line-scan crossing the red line in image (c) shows the surface profile. (For interpretation of the references to color in this figure legend, the reader is referred to the web version of this article.)

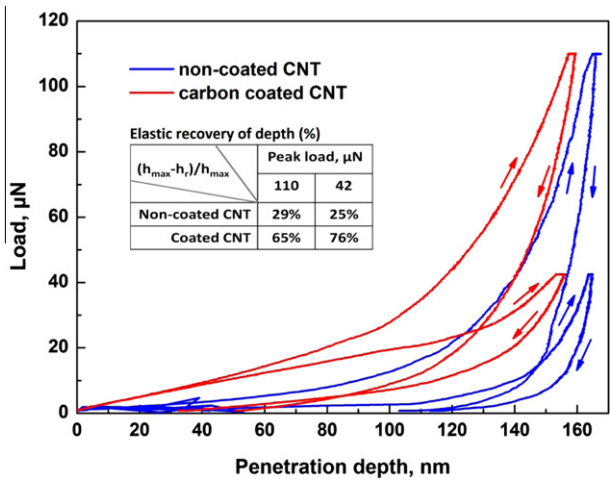

Fig. 11 – Loading/unloading curves of the carbon-coated (red) and non-coated (blue) SWCNT networks on silicon. The elastic recovery of indentation depth is calculated from maximum penetration depth, h_{max}, and residual depth, h_r. The coated SWCNT networks not only demonstrate higher resistance to the indenter penetration but also show larger elastic recovery. (For interpretation of the references to color in this figure legend, the reader is referred to the web version of this article.)

ing depth at maximum load, and h_r is the residual depth extracted from fitting the unloading data to a power-law equation following the Oliver and Pharr's method [22]. SPM images (Fig. 12) of the indented sites also proves the more elastic behavior of the coated network as the indentation left no recognizable mark on the sample surface (comparing Fig. 12a and b with 12c and 12d). This is in agreement with the SEM observation on the worn surface (Fig. 8) and suggests that the carbon-coated network had a rubber-like behavior in which the residual depths, h_r, could recover completely with time even at high peak-loads. The calculated ratio of depth recovery (Fig. 12e) gets close to 1 as the peak-load drops to 20 μN.

All of the above analysis suggests that under the nanowear conditions, the SWCNT bundles slid against each other with little resistance. The average depth of the worn area is about 60% of the original network thickness, indicating a possible higher adhesion of the SWCNT bundles to the substrate than the cohesion of the bundles as a network. On the other hand, the carbon coating not only reduced the amount of the deformation but also imparted elasticity to the SWCNT bundles as a whole. The results of the experiment indicate potentials of applying carbon coating on SWCNT network in developing conductive and transparent layers with enhanced resistance to contact pressure.

Fig. 13 shows the load-displacement curves from indenting the carbon coated and coating-free Si-surfaces for comparison. The different mechanical response of a 100 nm carbon coating and the Si substrate is clear. Under a peak-load of about 470 μN, the deformation in the carbon coating almost recovered completely with much higher hardness and elastic modulus values than that of the coating-free Si.

In summary, carbon coating significantly enhanced the integrity of the SWCNT network structure. Therefore, by applying carbon coatings on SWCNT networks, it is possible to develop novel conductive and transparent thin films with improved structural stability under contact pressure. Further experimental work is required in order to fully demonstrate the application potential of the hybrid nanomaterial.

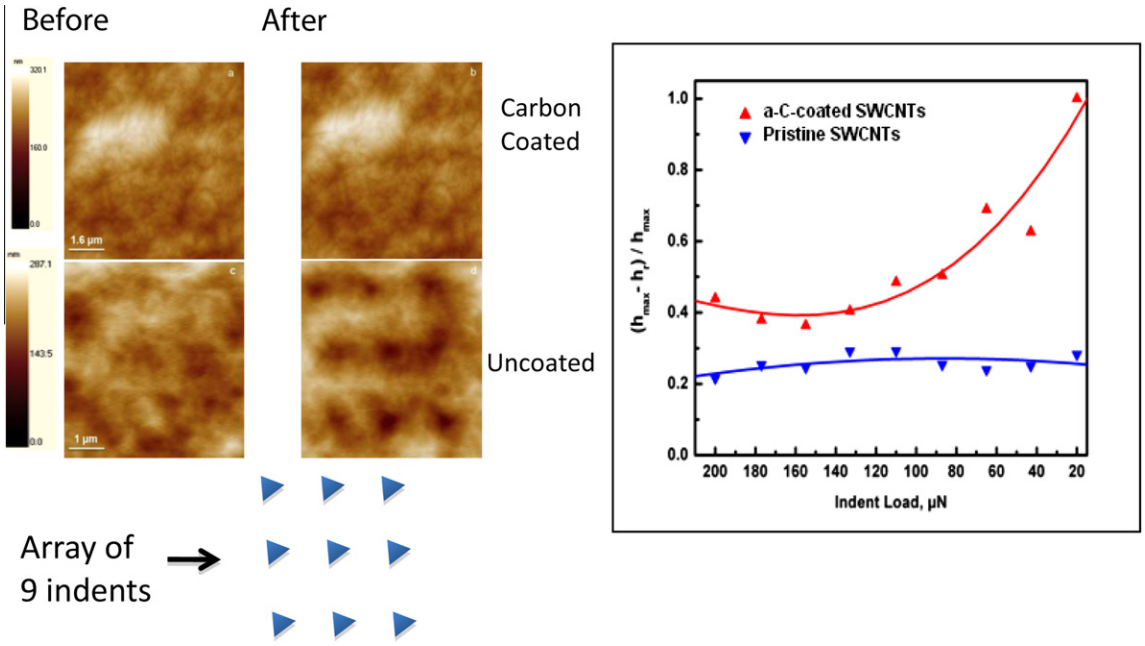

Fig. 12 – SPM images before and after indentation on: (a) and (b) the coated SWCNT network, and (c) and (d) the non-coated network. There are hardly any observable changes after the indentation on the surface of the coated networks. However, the 9 indent marks are clearly visible on the non-coated network surface. (e) The ratio of indentation depth recovery at each peak-load.

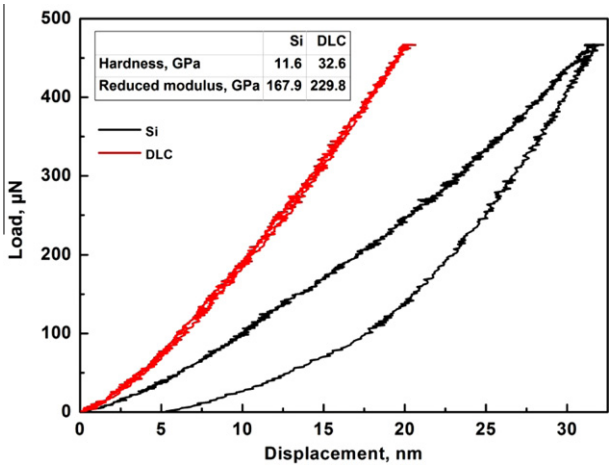

Fig. 13 – Plots of load *vs.* displacement on a 100 nm thick carbon coating on the Si wafer (red) and the coating-free substrate (black). (For interpretation of the references to color in this figure legend, the reader is referred to the web version of this article.)

4. Conclusions

To conclude, novel carbon-coated SWCNT network hybrid nanostructures were synthesized with PVD and characterized in detail for the first time with a multimodal approach including high resolution TEM. The experimental evidence from electron microscopy, optical spectroscopy and *in situ* electrical conductivity measurements indicates that SWCNTs are preserved during the energetic PVD process despite the structural modification of the surface layers of the material during the carbon coating process. The bonding configuration of the carbon coating observable on small diameter SWCNT bundles is drastically different than when the same coating process parameters are applied on a macroscopic substrate material, with dominantly graphitic instead of diamond-like composition. Poor thermal coupling between the nanostructures and the macroscopic substrate may lead to significant heating of the hybrid structure during the ion bombardment, which can lead to a subsequent relaxation of the sp^3 bonding to energetically more favorable sp^2 bonding. As exact determination bonding fractions is challenging due to partially overlapping EELS signals and has to be further studied in future experiments. However, the carbon coatings significantly reduce the permanent deformation in the hybrid nanomaterial compared to pristine networks, indicating improved mechanical properties i.e. improved elasticity of the material and better nanowear resistance at the selected loads and further experimental work is planned to expand the load range of mechanical testing. Further PVD process optimization will be carried out to reduce the ion flux and resulting heating, which should help to increase the sp^3-bonded carbon content. This may lead to an ultimate hybrid nanomaterial combining the electrical conductivity of SWCNT networks to the mechanical durability and insulating properties of DLC thin films.

Acknowledgements

This research was supported by the MIDE program of Aalto University. Special thanks for Petri Hirvonen for performing the temperature calculations.

REFERENCES

[1] Hannula SP, Koskinen J, Haimi E, Nowak R. Mechanical properties of nanostructured materials. In: Nalwa HS, editor. Encyclopedia of nanoscience and nanotechnology, vol. 5. California, USA: American Scientific Publishers; 2004. p. 131–62.
[2] Zhou XJ, Park JY, Huang S, Liu J, McEuen PL. Band structure, phonon scattering, and the performance limit of single-walled carbon nanotube transistors. Phys Rev Lett 2005;95(14):146805 1–4.
[3] Yao Z, Kane CL, Dekker C. High-field electrical transport in single-walled carbon nanotubes. Phys Rev Lett 2000;84(13):2941–4.
[4] Yu MF, Lourie O, Dyer MJ, Moloni K, Kelly TF, Ruoff RS. Strength and breaking mechanism of multiwalled carbon nanotubes under tensile load. Science 2000;287(5453):637–41.
[5] Treacy MMJ, Ebbesen TB, Gibson JM. Exceptionally high Young's modulus observed for individual carbon nanotubes. Nature 1996;381:678–80.
[6] Kaskela A, Nasibulin AG, Timmermans MY, Aitchison B, Papadimitratos A, Tian Y, et al. Aerosol-synthesized SWCNT networks with tunable conductivity and transparency by a dry transfer technique. Nano Lett 2010;10. 4349-4255.
[7] Nasibulin AG, Kaskela A, Mustonen K, Anisimov AS, Ruiz V, Kivistö S, et al. Multifunctional free-standing single-walled carbon nanotube films. ACS Nano 2011;5(4):3214–21.
[8] Segal M. Selling graphene by the ton. Nat Nanotechnol 2009;4:612–4.
[9] Shim BS, Zhu J, Jan E, Critchley K, Kotov NA. Transparent conductors from layer-by-layer assembled SWCNT films: importance of mechanical properties and a new figure of merit. ACS Nano 2010;4(7):3725–34.
[10] Sreekumar TV, Kumar S, Ericson LM, Hauge RH, Smalley RE. Single-wall carbon nanotube films. Chem Mater 2003;15:175–8.
[11] Donnet C, Erdemir A. Tribology of diamond-like carbon films. USA: Springer; 2008.
[12] Kinoshita H, Ippei I, Sakai H, Ohmae N. Synthesis and mechanical properties of carbon nanotube/diamond-like carbon composite films. Diamond Relat Mater 2007;16(11):1940–4.
[13] Wei C, Wang CI, Tao FC, Ting K, Chang RC. The stress reduction effect by interlayer deposition of film thickness for diamond like carbon on rough surface. Diamond Relat Mater 2010;19(5–6):518–24.
[14] Schittenhelm H, Geohegan DB, Jellison GE, Puretzky AA, Lance MJ, Britt PF. Synthesis and characterization of single-walled carbon nanotube-amorphous diamond thin-film composites. Appl Phys Lett 2002;81(11):2097–100.
[15] Moisala A, Nasibulin AG, Brown DP, Jiang H, Khriachtchev L, Kauppinen EI. Single-walled carbon nanotube synthesis using ferrocene and iron pentacarbonyl in a laminar flow reactor. Chem Eng Sci 2006;61(13):4393–402.
[16] Gonzalez D, Nasibulin AG, Shandakov SD, Queipo P, Jiang H, Kauppinen EI. Single-walled carbon nanotube charging during bundling process in the gas phase. Phys Status Solidi B 2006;243:3234–7.

[17] Koskinen J, Hirvinen JP, Keränen J. Effect of deposition temperature and growth rate on the bond structure of hydrogen free carbon films. J Appl Phys 1997;84(1):648–50.
[18] Witke T, Schuelke B, Schultrich B, Siemroth P, Vetter J. Comparison of filtered high-current pulsed arc deposition with conventional vacuum arc methods. Surf Coat Technol 2000;81(1):81–8.
[19] Robertson J. Diamond-like amorphous carbon. Mater Sci Eng R 2002;37:129–281.
[20] Pop E, Mann D, Wang Q, Goodson K, Dai H. Thermal conductance of an individual single-wall carbon nanotube above room temperature. Nano Lett 2005;6(1):96–100.
[21] Laurila T. et al. to be published.
[22] Varshney D, Weiner BR, Morell G. Growth and field emission study of a monolithic carbon nanotube/diamond composite. Carbon 2010;48(12):3359–63.